Characterization of the quasi-one-dimensional compounds δ-(EDT-TTF-CONMe2)2X, X=AsF6 and Br by vibrational spectroscopy and density functional theory calculations

Tobias Peterseim, Ágnes Antal, Martin Dressel, Patrick Batail, Natalia Drichko

AIP | The Journal of Chemical Physics

Characterization of the quasi-one-dimensional compounds δ-(EDT-TTF-CONMe2)2 X, X=AsF6 and Br by vibrational spectroscopy and density functional theory calculations

Tobias Peterseim, Ágnes Antal, Martin Dressel, Patrick Batail, and Natalia Drichko

Citation: The Journal of Chemical Physics **140**, 064504 (2014); doi: 10.1063/1.4865106
View online: http://dx.doi.org/10.1063/1.4865106
View Table of Contents: http://scitation.aip.org/content/aip/journal/jcp/140/6?ver=pdfcov
Published by the AIP Publishing

Characterization of the quasi-one-dimensional compounds δ-(EDT-TTF-CONMe$_2$)$_2X$, X=AsF$_6$ and Br by vibrational spectroscopy and density functional theory calculations

Tobias Peterseim,[1] Ágnes Antal,[1,2] Martin Dressel,[1] Patrick Batail,[3] and Natalia Drichko[1,4]
[1]*1. Physikalisches Institut, Universität Stuttgart, Pfaffenwaldring 57, 70550 Stuttgart, Germany*
[2]*Institute of Condensed Matter Physics, École Polytechnique Fédérale de Lausanne (EPFL), 1015 Lausanne, Switzerland*
[3]*Laboratoire MOLTECH, UMR 6200 CNRS-Université d'Angers, Bt. K, UFR Sciences, 2 Boulevard Lavoisier, F-49045 Angers, France*
[4]*Department of Physics and Astronomy, Johns Hopkins University, Baltimore, Maryland 21218, USA*

(Received 17 December 2013; accepted 27 January 2014; published online 12 February 2014)

We have investigated the infrared spectra of the quarter-filled charge-ordered insulators δ-(EDT-TTF-CONMe$_2$)$_2X$ (X= AsF$_6$, Br) along all three crystallographic directions in the temperature range from 300 to 10 K. DFT-assisted normal mode analysis of the neutral and ionic EDT-TTF-CONMe$_2$ molecule allows us to assign the experimentally observed intramolecular modes and to obtain relevant information on the charge ordering and intramolecular interactions. From frequencies of charge-sensitive vibrations we deduce that the charge-ordered state is already present at room temperature and does not change on cooling, in agreement with previous NMR measurements. The spectra taken along the stacking direction clearly show features of vibrational overtones excited due to the anharmonic electronic molecule potential caused by the large charge disproportionation between the molecular sites. The shift of certain vibrational modes indicates the onset of the structural transition below 200 K. © *2014 AIP Publishing LLC*. [http://dx.doi.org/10.1063/1.4865106]

I. INTRODUCTION

The physical properties of low-dimensional materials with strong electron-electron correlations, including organic conductors, can be essentially controlled by tuning the on-site Coulomb repulsion U, the nearest-neighbor interaction V, and the transfer integral t. Depending on the ratio, U/t or V/t and the bandfilling, a metal-insulator transition (MIT) can be observed in several different material classes,[1] for instance, transition-metal oxides, cuprates and molecular conductors, attracting more attention with respect to possible applications in future devices.[2,3] One possible reason for MIT to occur is the opening of a Mott gap due to the charge localization triggered by a large U/t ratio or second the localization of the carriers on different sites because of a large V/t, the so-called charged-ordered state.

One of the most prominent examples of a MIT is the organic one-dimensional Fabre salts, (TMTTF)$_2X$ (X=TaF$_6$, SbF$_6$, AsF$_6$, PF$_6$, ClO$_4$, Br, etc.), exhibiting a transition from a bad metal (semiconducting), half-filled dimerized state into an insulating charge-ordered one. The transition temperature can be tuned by chemical or hydrostatic pressure.[4,5] A deeper understanding of the charge ordering and its driving force will shed new light on the development of chemically tailored compounds and possible functional molecular devices. There is an ongoing discussion if the dimerization and hence the $\frac{1}{2}$ Umklapp scattering cause or destabilize the charge ordering.[6–8] Therefore it is of importance to study pure quarter-filled systems, where the dimerization between the molecular sites and, respectively, the $\frac{1}{2}$ Umklapp-scattering process are absent. This task was finally achieved in 2003 when the compounds δ-[(EDT-TTF)-CONMe$_2$]$_2$AsF$_6$ and δ-(EDT-TTF-CONMe$_2$)$_2$Br were synthesized.[9,10] These quasi-one-dimensional compounds δ-(EDT-TTF-CONMe$_2$)$_2X$, X=Br, and AsF$_6$ (abbreviated as EDT$_2$AsF$_6$ and EDT$_2$Br, respectively) exhibit an orthorhombic structure with the space group P_{2nn} at room temperature and undergo a structural second-order phase transition at 190 K into a $P2_1/a$ monoclinic crystal structure.[10] From a stoichiometric point of view, each molecular site carries a charge of $+0.5\,e$ leading to a quarter-filled band, but C^{13} NMR and x-ray[10,11] diffraction experiments reveal a charge-ordered state for both compounds which is established already at room temperature. The charge disproportionation derived from the NMR spin-lattice relaxation rate is as high as 1:9 for a ratio of charges on two neighboring molecular sites. The charge imbalance persists down to 10 K for both systems explaining their insulating behavior. The charges are arranged in an alternating way along all three crystallographic directions resulting in a three-dimensional pattern. The substitution of AsF$_6$ anion by Br is equivalent to an applied hydrostatic pressure of 7 kbar.[11] The p-T phase diagram based on pressure-dependent NMR and transport data has similarities to the well-established diagram of the (TMTTF)$_2X$ (X = TaF$_6$, SbF$_6$, AsF$_6$, PF$_6$, Br, and ClO$_4$ with M = S or Se) family.[4] Recently, Antal *et al.*[12] have investigated optical spectra of EDT$_2$AsF$_6$ and EDT$_2$Br. Along the stacking direction in the mid-infrared range we observed a broad band associated with the excitation of domain walls in the charge ordered state.[13]

The aim of this work is to gain more information on these compounds from the results of vibrational spectroscopy. Of particular interest is the charge imbalance between the

different molecular sites in the unit cell at various temperatures. We also trace possible structural changes on cooling, and get information about the interactions between the different molecular components in the crystal. To address these problems, we utilize infrared spectroscopy because it is one of the most powerful tools to study the charge distribution on the lattice in organic conductors, as well as the different coupling mechanisms between the intra- and intermolecular vibrations and the electronic system in these materials.[14] Here, we investigate the two compounds, EDT_2Br and EDT_2AsF_6, by comparing infrared spectra measured at temperatures between 300 K and 10 K for the three crystallographic axes with the results of *ab initio* quantum-mechanical calculations. The experimentally resolved vibrational modes are assigned with the help of the calculated frequencies of the normal modes for the cation and the neutral molecule of EDT-TTF-$CONMe_2$.

II. EXPERIMENTAL AND COMPUTATIONAL DETAILS

Reflectivity measurements on single crystals of EDT_2Br and EDT_2AsF_6 were performed in the spectral range between 600 cm^{-1} and 7000 cm^{-1} by using a Bruker IFS 66v and a Vertex 80v spectrometer equipped with a Hyperion microscope, purged by nitrogen gas to suppress the influence of the H_2O and CO_2 vibrational bands. The measurements have been conducted at temperatures between 300 and 10 K. The needle-like single crystals were grown by the method described in Refs. 9 and 10. The largest dimension of the crystals of about 1 mm is parallel to the *a*-axis; parallel to *b* the crystals have a width of about 0.1 mm, and parallel to *c*-axis, the height is around 0.05 mm. Samples were oriented at room temperature by measuring a polarization dependence of the IR spectra. For EDT_2Br, the polarized spectra have been recorded for the (*ab*) plane and for EDT_2AsF_6, all three crystallographic axes have been measured. The conductivity spectra of both compounds were calculated by Kramers-Kronig transformation. As the compounds are insulators at all measured temperatures, the reflectivity was extrapolated by a constant to lower frequencies and for the high frequencies up to 500 000 cm^{-1} by $R(\omega) \sim \omega^{-4}$ for the low reflecting *b*- and *c*-direction and by $R(\omega) \sim \omega^{-2}$ for the *a*-direction, respectively.

We performed *ab initio* quantum chemical calculation on the level of density functional theory (DFT) implemented in the Gamess package[15,16] to assign the experimental vibrational modes of EDT-TTF-$CONMe_2$ molecule. For the structure optimization the initial geometry was taken from the published x-ray data[10] for the isolated neutral molecule as well as for the cation. Due to the C_1 symmetry of the molecule all non-degenerated 84 vibrational modes are both Raman and infrared active. We used the hybrid B3LYP-functional[17] together with the basis set 6-31G(d) for the optimization procedure as well as for the normal mode analysis. An absence of imaginary frequencies in the calculations for both charge states was taken as an evidence that the equilibrium geometry was reached. To compare our calculated values with the experimental ones, we applied two different scaling factors, for the high-frequency vibrations 0.9679 (above 1300 cm^{-1}) and for the low-frequency modes 1.01, which has been actually determined for the triple-ζ basis set 6-311+G(d,p),[18] that yield in general satisfying agreement with the experimental results.[19,20]

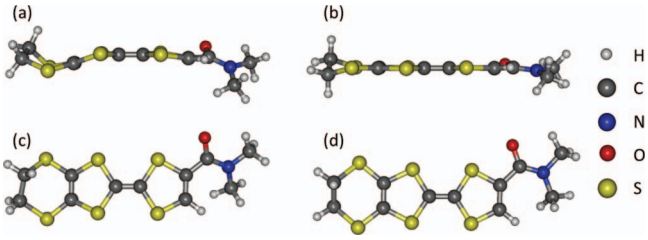

FIG. 1. (a) S-shaped equilibrium geometry of the neutral EDT-TTF-$CONMe_2$ molecule. (b) The optimized structure of the ionic EDT-TTF-$CONMe_2$ is planar in comparison to the neutral one. (c) and (d) corresponding top view of the neutral and cation structure.

III. RESULTS AND DISCUSSION

A. The neutral and positive charged EDT-TTF-$CONMe_2$ molecule

For the neutral molecule the geometry of relaxed ground state is distorted and boat-like; on the other hand the cation is flat as depicted in Fig. 1. Similar observations were made for several other organic molecules, for example, TMTTF, DMTTF, and BEDT-TTF.[20–24] For the inner C=C bond we calculated a length of 1.350 and 1.391 Å for the neutral and charged molecule, respectively, which is in very good agreement with the values of 1.354 and 1.392 Å determined experimentally.[10] X-ray results[10] reveal that the ethylene and methyl groups of the EDT-TTF-$CONMe_2$ possess two different configurations at room temperature. This matches with the calculation results, which suggest different configurations of these groups for the neutral and positively charged EDT-TTF-$CONMe_2$ molecule (see Figs. 1(a) and 1(b)). Apparently, the two different configurations of the ethylene and methyl groups belong to the molecules with different charges, in agreement with the suggestion that EDT_2Br and EDT_2AsF_6 are in the charge-ordered state at ambient conditions. At lower temperatures the two molecular configurations compete due to the charge imbalance. The decreasing molecular distance hampers the molecules to capture the two possible configurations and accordingly, structural methods cannot detect them.

B. Vibrational spectra in the direction perpendicular to the stacks

The maximum overlap between orbitals of EDT-TTF-$CONMe_2$ molecules occurs in stacking direction (*a*-axis). The spectra with light polarized along this direction mainly deliver information about the electronic excitations[12] which is reflected in the high optical conductivity in the *a*-direction of both compounds, as presented in Fig. 5.

The low reflectivity and conductivity of the *b*- and *c*-axes evidence the one-dimensional nature of the electronic system of the (EDT-TTF)-$CONMe_2$ family. The spectra polarized in this direction yield important information about the vibrational modes (see Figs. 2(a) and 2(b)), the charge state

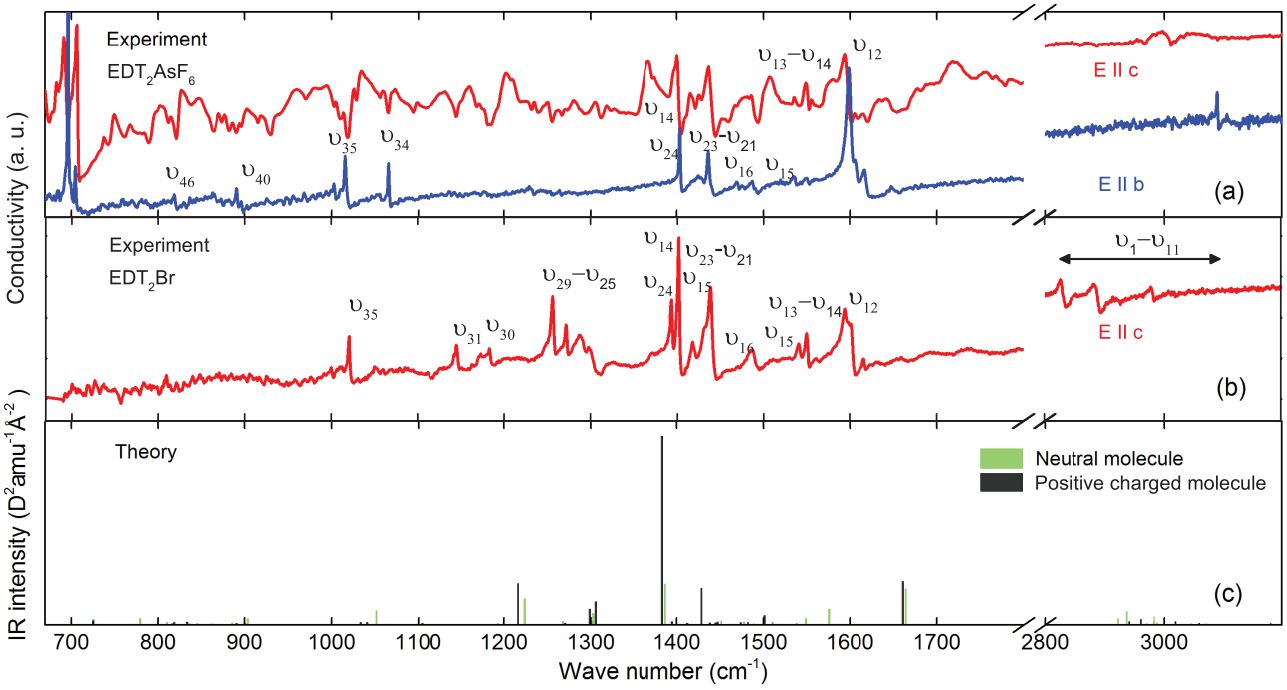

FIG. 2. Conductivity spectra of (a) EDT_2AsF_6 parallel to the *c*-axis at $T = 12$ K (red curve) and *b*-axis at 8 K (blue curve), (b) EDT_2Br parallel to the *c*-axis at 10 K, (c) the calculated resonance frequencies and intensities for the neutral molecule (light green bars) and the cation (black bars).

of the molecular sites, and the interaction of (EDT-TTF)-$CONMe_2$ molecules with the crystal environment. In Fig. 2, the low temperature conductivity spectra of EDT_2AsF_6 measured for the *c*- and *b*-directions are presented together with the conductivity spectra of EDT_2Br along the *c*-direction. These experimental data are compared with the calculated vibrational frequencies of the cation and the neutral EDT-$TTFCONMe_2$ molecule, plotted in Fig. 2(c).

As aforementioned in Sec. II, the molecules obey the C_1 symmetry leading to 84 vibrational modes which are both infrared and Raman-active. The intensities and resonance frequencies of the calculated modes of the cation and neutral molecule agree well with the ones observed experimentally, see Table I.

One of the most intense bands is the ν_{12} mode located at around 1600 cm^{-1}; it involves the stretching of the C=O bond. The band shows a splitting of 6 cm^{-1} for EDT_2AsF_6 and of 8 cm^{-1} for EDT_2Br which can be observed only at temperatures below 100 K. The splitting is caused by unequal charge on two donor molecules. At higher temperatures the splitting is not resolved due to the large bandwidth (9 cm^{-1}) of this feature.

The modes most sensitive to the molecular ionicity are those modes which include the vibration of C=C double bonds. In several compounds originating from the TTF family,[25] for example, TMTTF[20,26] and BEDT-TTF,[14] a linear dependence is observed between the frequency shift and the charge per molecule; this holds mainly for modes which are not subject to electron-molecular-vibrational (emv-) coupling.[27,28] Our calculations reveal several modes that exhibit a distinct frequency shift when the ionicity of the (EDT-TTF)-$CONMe_2$ molecule changes. With the charge on the molecule decreasing from 0 to $+1e$ the ν_{13}, ν_{14}, and ν_{15} modes shift down in frequency by about 40, 165, and 82 cm^{-1}, respectively. Based on the ν_{14} and ν_{15} frequencies observed in the spectra for $E \parallel c$, we could estimate values for the charge disproportionation between two different molecular sites of about 0.8 and 0.82*e* for EDT_2AsF_6, and 0.82 and 0.75*e* for EDT_2Br, respectively. The small discrepancy between the results received using different vibrations arises from the fact that these vibrations can couple to the electronic background (emv) and hence the original relation between ionicity and frequency shift is slightly altered. In addition, the ν_{15} mode involves the bending of the H–C–H bonds of the methyl groups and thus is sensitive to thermal contraction as obvious from Figs. 3(a) and 3(b). As a whole, our results agree well with previous NMR experiments[10] which concluded a charge imbalance of 9:1 for both compounds. Our measurements also could not resolve any redistribution of the charge below $T = 200$ K for EDT_2AsF_6 and below 150 K for EDT_2Br.

C. Temperature-dependent behavior of the optical response perpendicular to the stacking direction

On cooling, most vibrational bands slightly shift to higher frequencies due to the thermal contraction of the crystal, and their linewidth decreases. The largest changes with temperature are observed for the ν_{15} and ν_{21} bands in the *c*-direction; these modes are related to the bending of the H–C–H bonds in the CH_3 group. In Fig. 3 *c*-direction conductivity of EDT_2AsF_6 and EDT_2Br is plotted for various temperatures. There, several modes undergo a significant shift upon cooling. In order to analyze the changes more quantitatively, we fitted the vibrational modes for all temperatures.

TABLE I. Calculated frequencies (in cm^{-1}) and infrared intensities (given in units of $D^2amu^{-1}Å^{-2}$). The direction of observation is noted in brackets behind the experimental values. The following abbreviations are used: Int.: Intensity, asym: asymmetric, sym: symmetric, def: deformation, ip: in-plane, oop: out-of-plane, tor: torsion, str: stretching, brea: breathing, bend: bending, wag: wagging, rock: rocking.

	EDT_2AsF_6	EDT_2Br	(EDT-TTF)-$CONMe_2^0$			(EDT-TTF)-$CONMe_2^+$			
Label	Experimental	Experimental	ν_{calc}	ν_{scaled}	Int.	ν_{calc}	ν_{scaled}	Int.	Mode description
ν_1			3249	3145	0.037	3283	3177	0.271	C–H str, asym
ν_2	…	…	3196	3094	0.025	3209	3106	0.018	C–H str, asym
ν_3	…	…	3171	3069	0.212	3160	3059	0.267	C–H str, asym
ν_4	…	…	3146	3045	0.181	3159	3058	0.005	C–H str, asym
ν_5	…	…	3128	3028	0.01	3148	3047	0.003	C–H str, asym
ν_6	…	…	3088	2989	0.358	3122	3022	0.084	C–H str, asym
ν_7	3011(*c*)	2980 (*c*)	3083	2984	1.326	3120	3019	0.581	C–H str, asym
ν_8	…	…	3082	2983	0.562	3095	2995	0.017	C–H str, sym
ν_9	…	…	3070	2972	0.308	3091	2992	0.036	C–H str, sym
ν_{10}	…	2890 (*c*)	3036	2938	2.16	3060	2962	0.941	C–H str, sym
ν_{11}	…	2830 (*c*)	3021	2924	1.027	3040	2942	0.537	C–H str, sym
ν_{12}	1599/1605 (*b,c*)	1592/1600 (*c*)	1720	1664	5.939	1716	1661	7.101	C=O str
ν_{13}	1551(*c*)	1549 (*c*)	1628	1576	2.62	1589	1538	0.233	C=C str
ν_{14}	1536/1404 (*c*)	1538/1403 (*c*)	1601	1549	1.041	1430	1384	31.029	C=C str
ν_{15}	1488/1421 (*b,c*)	1490/1428 (*c*)	1561	1511	0.412	1476	1429	5.98	H–C–H bend, asym, C=C str
ν_{16}	…	…	1561	1511	0.434	1551	1502	1.57	H–C–H bend, asym, C=C str
ν_{17}	…	…	1539	1489	0.218	1535	1486	0.128	H–C–H bend, asym
ν_{18}	…	…	1527	1478	0.5	1532	1483	0.441	H–C–H bend, asym
ν_{19}	…	…	1523	1474	0.269	1523	1474	0.439	H–C–H bend, asym
ν_{20}	…	…	1509	1460	0.028	1493	1445	0.323	H–C–H bend, sym
ν_{21}	1438 (*b,c*)	1440 (*c*)	1500	1452	0.638	1496	1447	0.48	H–C–H bend, sym
ν_{22}	1419 (*b,c*)	1416 (*c*)	1482	1435	0.149	1487	1439	0.345	H–C–H bend, sym
ν_{23}	1409 (*c*)	1410 (*c*)	1460	1414	0.270	1459	1412	0.316	H–C–H bend, sym
ν_{24}	1396 (*b,c*)	1395 (*c*)	1433	1387	6.697	1441	1395	0.585	H–C–H bend, sym, C–N–C str
ν_{25}	…	1300 (*c*)	1345	1302	0.64	1349	1306	0.3805	CH_2 wag
ν_{26}	…	…	1310	1268	0.047	1326	1283	0.064	CH_2 wag
ν_{27}	…	1290 (*c*)	1290	1303	1.866	1286	1299	2.61	N–C–H bend, C–H bend
ν_{28}	…	1272 (*c*)	1255	1268	0.57	1258	1271	0.291	C–H bend
ν_{29}	…	1256 (*c*)	1212	1224	4.277	1204	1216	6.748	N–C–H bend, C–C str
ν_{30}	…	1173/1184 (*c*)	1206	1218	0.146	1230	1243	0.002	CH_2 wag
ν_{31}	…	1146 (*c*)	1181	1193	0.269	1174	1185	0.073	N–C–H bend
ν_{32}	…	…	1164	1175	0.073	1169	1181	0.037	CH_2 twi
ν_{33}	…	…	1149	1160	0.034	1134	1146	0.074	N–C–H bend
ν_{34}	1064 (*b*)	…	1098	1109	0.163	1094	1105	0.288	N–C–H bend
ν_{35}	1015/1002 (*b,c*)	1020/1000 (*c*)	1042	1052	2.292	1032	1041	0.431	N–C–H bend
ν_{36}	…	…	1027	1037	0.021	1020	1030	0.09	CH_2–CH_2 str
ν_{37}	1000 (*b,c*)	1000 (*c*)	1007	1017	0.021	1024	1034	0.4	CH_2–CH_2 str
ν_{38}	…	…	983	992	0.001	1048	1059	0.068	S–C–S str
ν_{39}	…	…	973	983	0.129	950	959	0.157	CH_2 rock
ν_{40}	896/891 (*b*)	…	895	904	1.06	891	899	0.0001	S–C bend, CH_2 rock
ν_{41}	…	…	877	886	0.367	882	891	0.2489	N–CH_3 bend, C–H bend
ν_{42}	…	…	853	862	0.245	912	921	0.087	S–C str, CH_2 rock
ν_{43}	…	…	837	845	0.256	892	901	0.235	S–C str
ν_{44}	…	…	829	837	0.221	825	834	0.476	S–C bend, N–CH_3 str
ν_{45}	…	…	802	810	0.425	808	816	0.223	C–H bend
ν_{46}	819 (*b*)	…	771	779	1.034	811	819	0.397	S–C bend
ν_{47}	…	…	768	776	0.054	791	799	0.057	S–C–S bend
ν_{48}	719 (*a*)	714 (*a*)	719	726	0.948	719	726	0.671	O–C–C bend
ν_{49}	…	…	709	716	0.163	712	719	0.029	S–C str
ν_{50}	…	…	671	677	0.062	677	684	0.042	S–CH_2 str
ν_{51}	…	…	641	647	0.516	647	653	0.881	ip ring def, N–C–O bend
ν_{52}	…	…	617	623	0.075	640	646	0.0228	ip ring def
ν_{53}	…	…	550	556	0.024	524	529	0.0272	oop ring def
ν_{54}	…	…	524	529	0.299	524	529	0.013	oop ring def
ν_{55}	…	…	508	513	0.019	499	504	0.072	N–CH_3 sci, ip ring def
ν_{56}	…	…	483	488	0.023	509	514	0.011	ip ring def
ν_{57}	…	…	461	465	0.022	474	479	0.003	ip ring def

TABLE II. (*Continued.*)

Label	EDT_2AsF_6 Experimental	EDT_2Br Experimental	(EDT-TTF)-$CONMe_2^0$			(EDT-TTF)-$CONMe_2^+$			Mode description
			ν_{calc}	ν_{scaled}	Int.	ν_{calc}	ν_{scaled}	Int.	
ν_{58}	...	...	452	456	0.093	477	481	0.746	ip ring def
ν_{59}	...	...	444	448	0.061	453	458	0.036	N–CH_3 sci
ν_{60}	...	...	418	422	0.133	433	438	0.009	ip ring def
ν_{61}	...	...	408	412	0.407	413	417	0.676	N–CH_3 sci
ν_{62}	...	...	369	373	0.007	357	361	0.003	ip ring def
ν_{63}	...	...	349	352	0.012	342	346	0.192	ip rings def
ν_{64}	...	...	340	343	0.07	333	3336	0.001	ip rings def
ν_{65}	...	...	332	335	0.085	297	300	0.173	CH_3 rock
ν_{66}	...	...	309	312	0.007	311	314	0.044	CH_3 rock
ν_{67}	...	...	272	274	0.008	314	317	0.048	oop def
ν_{68}	...	...	265	267	0.027	271	274	0.01	oop def
ν_{69}	...	...	251	254	0.205	279	282	0.351	CH_3 rock
ν_{70}	...	...	250	253	0.104	264	266	0.021	CH_3 rock
ν_{71}	...	...	227	229	0.061	231	233	0.117	ip def
ν_{72}	...	...	195	197	0.03	219	221	0.049	oop def
ν_{73}	...	...	177	179	0.011	193	195	0.015	oop def
ν_{74}	...	...	154	156	0.028	161	163	0.006	ip def
ν_{75}	...	...	140	141	0.023	141	143	0.162	ip def
ν_{76}	...	...	132	134	0.006	127	129	0.007	oop def
ν_{77}	...	...	117	118	0.023	100	101	0.001	oop def
ν_{78}	...	...	91	92	0.039	106	107	0.02	oop def
ν_{79}	...	...	76	77	0.009	65	65	0.012	oop def
ν_{80}	...	...	67	68	0.066	54	54	0.007	def
ν_{81}	...	...	52	52	0.064	46	47	0.117	def
ν_{82}	...	...	41	42	0.058	48	49	0.051	oop def
ν_{83}	...	...	38	38	0.011	33	33	0.061	oop def
ν_{84}	...	...	18	18	0.068	24	25	0.006	oop def, boat mode

As we cannot exclude a presence of weak coupling of the out-of-plane vibrational modes to the electronic background, we utilized the Fano model[29] to describe the partially asymmetric features. The temperature dependence of the ν_{15}, ν_{21}, ν_{22}, and ν_{23} resonance frequencies is displayed in Fig. 4. At $T = 200$ K the ν_{21} mode is located at 1430 cm^{-1} for EDT_2AsF_6 and at 1435 cm^{-1} for EDT_2Br. Upon cooling further, the modes move towards higher frequencies by about 9 cm^{-1} for EDT_2AsF_6 and 5 cm^{-1} for EDT_2Br, respectively. The ν_{15} behaves in a similar way and can be observed at 1421 cm^{-1} and at 1428 cm^{-1}; the shift is about 5 cm^{-1}. As mentioned before,[10] EDT_2Br undergos a second-order structural phase transition at $T_S = 190$ K where the unit cell parameter γ changes gradually from 90° to 92.45° when the temperature is reduced from 190 to 120 K. For EDT_2AsF_6 only the structure of the monoclinic phase at 100 K has been studied by x-ray; nevertheless, ESR investigations could detect a change in the linewidth and spin-susceptibility at $T_S \approx 190$ K which is associated with a similar structural transition. According to our observations, the vibrational modes start to harden below 200 K when the structural transition sets in and saturate below 100 K. This can be an evidence that at the structural phase transition the molecular cavity which contains the counter ion and is formed by the ethylene and methyl groups is modified. This conclusion agrees with structural studies, which show that the distance of C_{Me}–H ⋯ Br (see Fig. 4(b)) in the case of EDT_2Br diminishes below the structural transition and the angles between the entities C_{Me}–H ⋯ Br are strongly altered.[10] Our data suggest that EDT_2AsF_6 also undergoes a structural transition at about 200 K with structural changes similar to EDT_2Br.

D. Polarization parallel to the stacking direction

In Figs. 5(a) and 5(b) we present the temperature dependence of the conductivity spectra of EDT_2AsF_6 and EDT_2Br in the *a*-axis direction. The origin of the broad mid-infrared band that appears only in this polarization has been discussed in details in the Ref. 12. The band can be ascribed to optical excitations of domain walls in the charge-ordered state. Here we will focus on the fine structures superimposed on this mid-infrared band. In the case of EDT_2AsF_6, two strong sharp peaks at around 699 and 719 cm^{-1} (indicated by the diamond in Fig. 5) with satellite peaks located at 696 and 712 cm^{-1} are observed for all temperatures. The peak at 699 cm^{-1} agrees well with the frequency of the symmetric three-times degenerated $\nu_3(t_{1u})$ mode of the free AsF_6 molecule observed at 700 cm^{-1} in the gas phase.[30] In analogy to the one-dimensional Fabre-salt $(TMTTF)_2AsF_6$,[20] the degeneracy of the ν_3 is lifted due to the low crystal-site symmetry C_1 leading to three slightly separated peaks. The pattern does not undergo any redistribution with temperature. The feature observed at 719 cm^{-1} in EDT_2AsF_6 can also be found at 714 cm^{-1} in EDT_2Br. We assign this peak to the ν_{48}

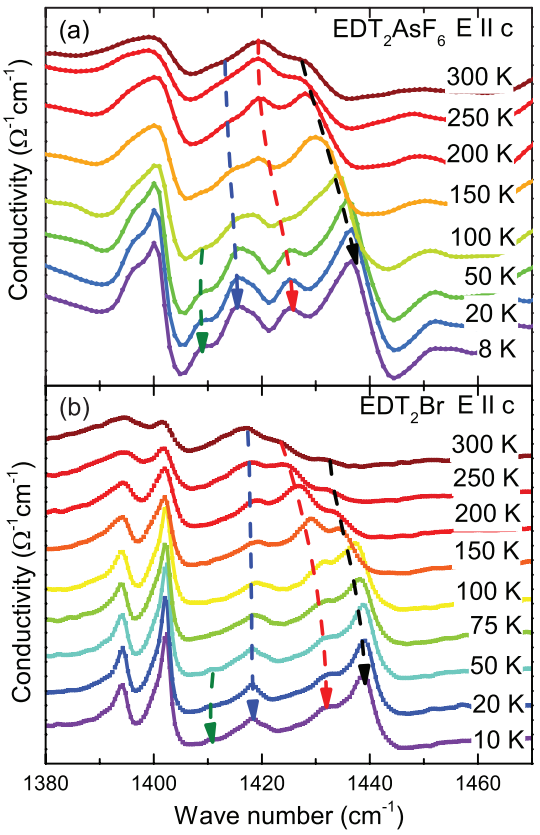

FIG. 3. The conductivity spectra of (a) EDT_2AsF_6 and (b) EDT_2Br in the region of the C–H vibrations recorded at different temperatures along the *c*-direction. The ν_{21} mode (black arrow) hardens on cooling and becomes sharper for both compounds. A similar behavior is found for the ν_{15} mode (red arrow) whereas ν_{22} (blue arrow) exhibits only a small softening for EDT_2AsF_6. The ν_{23} (olive arrow) becomes visible only below $T = 100$ K. For clarity, the spectra are shifted by a constant values with respect to each other.

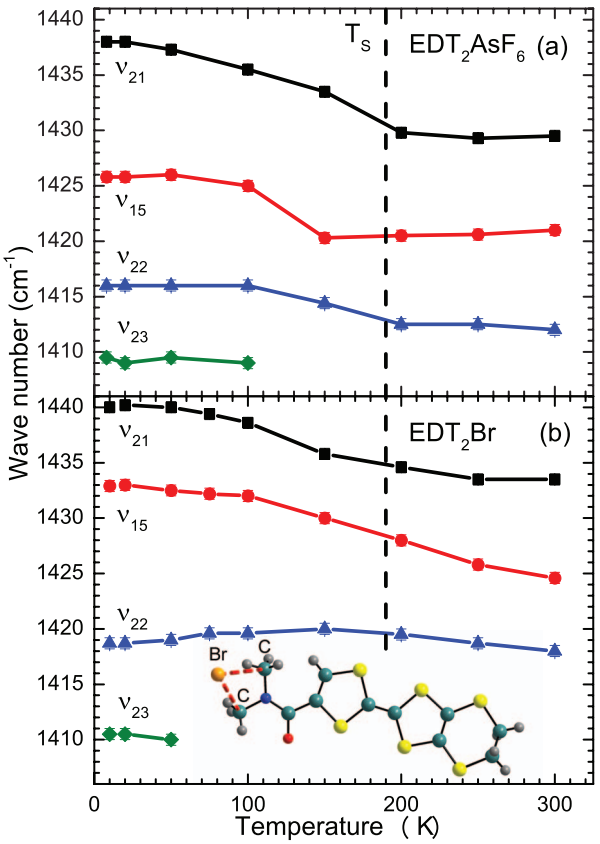

FIG. 4. (a) and (b) Temperature dependence of the resonance frequency of the ν_{21} (black), ν_{15} (red), ν_{22} (blue), and ν_{23} modes between 10 and 300 K. In both compounds the modes ν_{21} and ν_{15} shift to higher frequencies on cooling below the structural transition at $T_S = 190$ K which is marked by a dashed line. In the lower part of (b) the EDT-TTFCONMe$_2$ molecule and the anion Br are displayed.

out-of plane O–C–C bending mode. For EDT_2AsF_6 the experimental spectra at lower frequencies are obscured by the interference fringes and thus the analysis is not possible. In case of EDT_2Br, no sharp resonance peaks are visible in the low-frequency range.

For both compounds we find several antiresonance dips and asymmetric bands superimposed on the mid-infrared band; they are highlighted by the dashed lines in Fig. 5. Similar features have previously been observed in the spectra of other organic conductors; they mostly occur in compounds with a charge-ordered state, for instance, α-(BEDT-TTF)$_2$I$_3$,[31] Θ-(BEDT-TTF)$_2$RbZn(SCN)$_4$,[27] and the TMTTF$_2X$ (X=SbF$_6$, AsF$_6$, and PF$_6$) family.[20] Of particular importance are the antisymmetric modes at 1890 cm^{-1} and at 2880 cm^{-1} for EDT_2AsF_6 and EDT_2Br, respectively, which cannot be assigned to any fundamental vibrational mode according to our normal mode analysis.

Recently, Yamamoto *et al.*[32] explained this phenomenon by using a simple model system which consists of two molecules forming a dimer. They calculated the emv-coupling of the molecular modes to the electronic continuum and extended the linear-coupling theory[33] to higher order with nonlinear terms representing the anharmonic electronic potential. As a result overtones appear in the calculated spectra. Two dominant parameters, called A_{CT} and A_{CD}, can be found in the higher order terms. The first one

$$A_{CT} = \left| \frac{g g^{(2)} \delta n_{eg}^2}{\sqrt{2} E_{eg}} \right| \quad (1)$$

accounts for the enhancement of the anharmonicity of the molecular potential due to the charge transfer between the two molecular sites; therefore it depends on the transfer matrix element δn_{eg}. The second term

$$A_{CD} = \left| \frac{g^3 \delta n_{eg}^2 \delta\rho}{\sqrt{2} E_{eg}^2} \right| \quad (2)$$

depends on the charge imbalance $\delta\rho$ between the two molecules. Since both terms may be relevant at the same time, the overtones can be excited in a system where charge ordering is absent. The g parameter is the emv-coupling constant. For our estimation of the ratio A_{CD}/A_{CT}, we used $g = 132$ meV which is the value of the emv-coupling constant for the ν_3 (a_g) mode of BEDT-TTF molecule.[34] This is certainly a good approximation for the most important C=C modes that belong to the TTF skeleton also for (EDT-TTF)-CONMe$_2$. It is known, that for TTF-based molecules, the g values are rather similar; they increase slightly as the molecules get larger, from 117 meV for TTF,[35] to 120 meV for TMTTF,[36] and

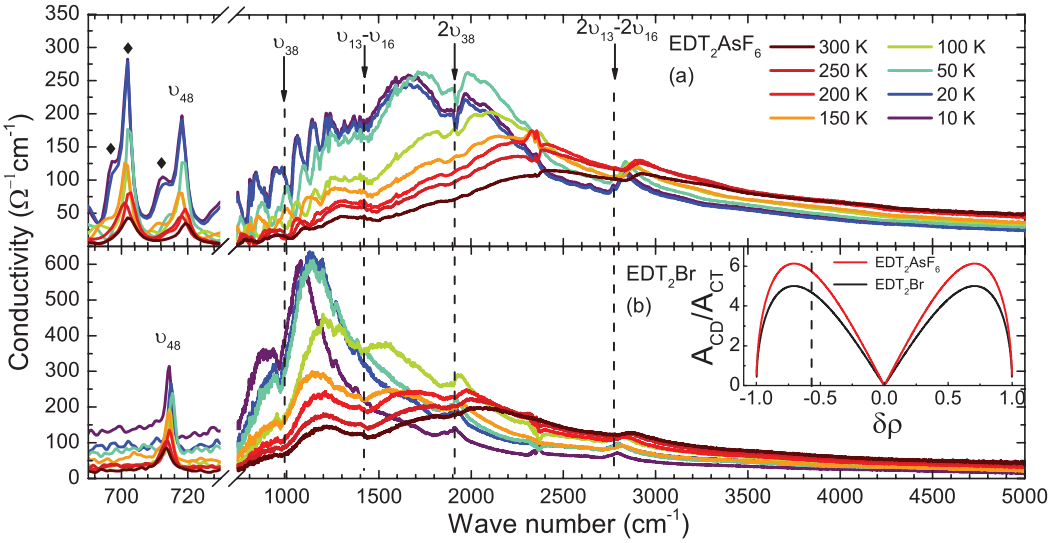

FIG. 5. Evolution of the *a*-axis conductivity of (a) EDT_2AsF_6, and (b) EDT_2Br in the temperature range from 300 K to 10 K. The dashed lines mark the fundamental emv-coupled modes, the second harmonic modes, and sum-frequencies, as indicated. The strong resonance peak at 702 cm^{-1} (marked by the black diamond) can be assigned to the ν_3 (t_{1u}) mode of EDT_2AsF_6. The inset in the lower panel exhibits the ratio between A_{CD} and A_{CT} as a function of the charge disproportionation $\delta\rho$ for the two compounds, EDT_2AsF_6 (red) and EDT_2Br (black).

132 meV for BEDT-TTF.[34] The quadratic coupling constant $g^{(2)}$ is the second derivative of the valance band E_g on the vibrational normal coordinate Q. It can be derived from the difference of the vibrational frequency between the cation (ω_{cat}) and neutral (ω_{neu}) molecule (for further explanation see Ref. 32):

$$g^{(2)} = \frac{1}{2}(\omega_{cat} - \omega_{neu}), \tag{3}$$

which is 10 meV in the case of the ν_{14} mode. The transfer matrix elements δn_{eg} and the energy gap E_{eg} can be expressed as

$$\delta n_{eg} = \sqrt{1 - \delta\rho^2}, \tag{4}$$

$$E_{eg} = \frac{2t_{\parallel}}{\sqrt{1 - \delta\rho^2}}. \tag{5}$$

The energy gap depends on the intrastack transfer integral $t_{\parallel}$, which has been calculated by the extended Hückel theory for EDT_2Br at 150 K to be 87 meV (Ref. 10) and for EDT_2AsF_6 at 300 K to be equal to 71 meV.[9] In the inset of Fig. 5 the ratio A_{CD}/A_{CT} is plotted as a function of the charge disproportionation $\delta\rho$. When the difference in charge becomes larger than $0.1e$ the A_{CD} term dominates significantly. For the two compounds under investigation, the charge imbalance $\delta\rho \approx 0.8e$, and the A_{CD}/A_{CT} ratio is close to its maximum; thus the overtones appear predominantly due to the charge ordering.

Based on our normal mode analysis summarized in Table I, we can now identify overtones of the vibrational modes, which appear in our spectra. The harmonic overtone located at 1970 cm^{-1} corresponds to ν_{38} with a fundamental frequency of 970 cm^{-1} (theoretical values: 992 cm^{-1} for the neutral molecule). The second dip at 2900 cm^{-1} is assigned to the overtones of the ν_{13}, ν_{14}, ν_{15}, and ν_{16} modes involving the C=C double bonds (theoretical values: 1576 cm^{-1}, 1549 cm^{-1}, 1511 cm^{-1}, and 1511 cm^{-1} for the neutral molecule).[23,30]

The antiresonance features of the overtones change their profile with decreasing temperature, following the shift of the position of the mid-infrared band maximum, as the shape of the emv-coupled modes depends on the relative position of the electronic maximum and the resonance frequency of the vibrational mode. The existence of the overtone resonances, being present already at room temperature, is a strong indicator of the charge-ordered state for both compounds.

IV. CONCLUSION

We have performed DFT calculations of the vibrational modes of the free neutral and charged EDT-TTF-CONMe$_2$ molecule and compared the results with optical spectra of EDT_2AsF_6 and EDT_2Br taken at different temperatures and directions of polarization. We made a detailed assignment of the vibrational modes. The behavior of specific modes supports our previous findings (Ref. 12) that the charge order state is stable in the compounds of the EDT-TTF-CONMe$_2$ family in the whole measured temperature range from 10 to 300 K with a rather large charge disproportionation of about $0.8e$. The change of the frequencies associated with vibrations of CH_3 groups below $T_S = 190$ K marks a structural transition for both compounds. The *a*-axis optical conductivity of both compounds reveals strong fingerprints of vibrational overtones which are strongly enhanced and activated by the charge disproportionation.

ACKNOWLEDGMENTS

We acknowledge valuable discussions with A. Girlando and A. Jánossy. We thank D. Wu and R. Beyer for technical help and for discussions. Á. Antal acknowledges the support

of DAAD, N. Drichko acknowledges a support of Margarete von Wrangell Habilitationstipendium and H. Blewett Fellowship. T. Peterseim appreciates the support of the Carl-Zeiss Stiftung. We would like to thank the bwGRiD for providing the computational resources and the Deutsche Forschungsgemeinschaft (DFG) for financial support.

[1]M. Imada, A. Fujimori, and Y. Tokura, Rev. Mod. Phys. **70**, 1039 (1998).
[2]F. Sawano, I. Terasaki, H. Mori, T. Mori, M. Watanabe, N. Ikeda, Y. Nogami, and Y. Noda, Nature **437**, 522 (2005).
[3]Z. Yang, C. Ko, and S. Ramanathan, Annu. Rev. Mater. Res. **41**, 337 (2011).
[4]M. Dressel, Naturwissenschaften **94**, 527 (2007).
[5]F. Iwase, K. Sugiura, K. Furukawa, and T. Nakamura, J. Phys. Soc. Jpn. **78**, 104717 (2009).
[6]T. Giamarchi, Physica B **230-232**, 975 (1997).
[7]V. Emery, R. Bruinsma, and S. Barišić, Phys. Rev. Lett. **48**, 1039 (1982).
[8]Y. Shibata, S. Nishimoto, and Y. Ohta, Phys. Rev. B **64**, 235107 (2001).
[9]K. Heuzé, M. Fourmigué, P. Batail, C. Coulon, R. Clérac, E. Canadell, P. Auban-Senzier, S. Ravy, and D. Jérome, Adv. Mater. **15**, 1251 (2003).
[10]L. Zorina, S. Simonov, C. Mézière, E. Canadell, S. Suh, S. E. Brown, P. Foury-Leylekian, P. Fertey, J.-P. Pouget, and P. Batail, J. Mater. Chem. **19**, 6980 (2009).
[11]P. Auban-Senzier, C. Pasquier, D. Jérome, S. Suh, S. Brown, C. Mézière, and P. Batail, Phys. Rev. Lett. **102**, 257001 (2009).
[12]Á. Antal, T. Knoblauch, M. Dressel, P. Batail, and N. Drichko, Phys. Rev. B **87**, 075118 (2013).
[13]M. Mayr and P. Horsch, Phys. Rev. B **73**, 195103 (2006).
[14]M. Dressel and N. Drichko, Chem. Rev. **104**, 5689 (2004).
[15]M. W. Schmidt, K. K. Baldridge, J. A. Boatz, S. T. Elbert, M. S. Gordon, J. H. Jensen, S. Koseki, N. Matsunaga, K. A. Nguyen, S. Su, T. L. Windus, M. Dupuis, and J. A. Montgomery, J. Comput. Chem. **14**, 1347 (1993).
[16]M. S. Gordon and M. W. Schmidt, *Theory and Applications of Computational Chemistry* (Elsevier, 2005), pp. 1167–1189.
[17]A. D. Becke, J. Chem. Phys. **98**, 5648 (1993).
[18]M. P. Andersson and P. Uvdal, J. Phys. Chem. A **109**, 2937 (2005).
[19]A. Girlando, J. Phys. Chem. C **115**, 19371 (2011).
[20]M. Dressel, M. Dumm, T. Knoblauch, and M. Masino, Crystals **2**, 528 (2012).
[21]D. Jankowski, R. Świetlik, E. W. Reinheimer, and M. Fourmigué, J. Raman Spectrosc. **42**, 1518 (2011).
[22]A. Łapiński, L. Ouahab, and T. Imakubo, Vib. Spectrosc. **52**, 22 (2010).
[23]A. Łapiński and A. Kotov, Chem. Phys. **326**, 551 (2006).
[24]E. Demiralp, S. Dasgupta, and W. A. Goddard, J. Am. Chem. Soc. **117**, 8154 (1995).
[25]R. Bozio, I. Zanon, A. Girlando, and C. Pecile, J. Chem. Phys. **71**, 2282 (1979).
[26]M. Meneghetti, R. Bozio, I. Zanon, C. Pecile, C. Ricotta, and M. Zanetti, J. Chem. Phys. **80**, 6210 (1984).
[27]K. Yamamoto, K. Yakushi, K. Miyagawa, K. Kanoda, and A. Kawamoto, Phys. Rev. B **65**, 085110 (2002).
[28]K. Yamamoto, T. Yamamoto, K. Yakushi, C. Pecile, and M. Meneghetti, Phys. Rev. B **71**, 045118 (2005).
[29]U. Fano, Phys. Rev. **124**, 1866 (1961).
[30]K. Nakamoto, *Infrared and Raman Spectra of Inorganic and Coordination Compounds*, 6th ed. (Wiley, Hoboken, NJ, 2009).
[31]T. Ivek, B. Korin-Hamzić, O. Milat, S. Tomić, C. Clauss, N. Drichko, D. Schweitzer, and M. Dressel, Phys. Rev. B **83**, 165128 (2011).
[32]K. Yamamoto, A. A. Kowalska, Y. Yue, and K. Yakushi, Phys. Rev. B **84**, 064306 (2011).
[33]M. Rice, V. Yartsev, and C. Jacobsen, Phys. Rev. B **21**, 3437 (1980).
[34]M. Kozlov, K. Pokhodnia, and A. Yurchenko, Spectrochim. Acta, Part A **45**, 437 (1989).
[35]R. Bozio and C. Pecile, J. Phys. C: Solid State Phys. **13**, 6205 (1980).
[36]D. Pedron, R. Bozio, M. Meneghetti, and C. Pecile, Mol. Cryst. Liq. Cryst. Sci. Technol., Sect. A **234**, 161 (1993).